Dispersion of the Magnon and Optical-Exciton States of $GdCl_3$ and $Gd(OH)_3$ and Their Effect upon the Single-Ion-Induced Absorption Line Shapes*

R. S. Meltzer
Department of Physics, University of Georgia, Athens, Georgia 30601
and Department of Physics, Johns Hopkins University, Baltimore, Maryland 21218

and

H. W. Moos
Department of Physics, Johns Hopkins University, Baltimore, Maryland 21218
(Received 7 February 1972)

The high-resolution optical-absorption spectra of the magnetic insulators $GdCl_3$ and $Gd(OH)_3$ in a 35-kG magnetic field are used to demonstrate, for the first time, the influence of the magnon dispersion on the line shapes of single-ion-induced optical transitions. The absorption line shapes for transitions from the first thermally populated spin state to several single-ion states of the $^6P_{7/2}$ and $^6P_{5/2}$ manifolds of the Gd^{+3} ion are calculated. The initial and final states are properly treated as a magnon and exciton, respectively, including the dispersion of both states. The single-ion transition-moment operator is transformed to a basis in the crystal eigenstates and the resulting absorption line shape is shown to depend on a $\vec{k}$-dependent transition-moment operator weighted by a combined exciton-magnon density of states and the magnon occupation number. The magnon dispersion is calculated from the known ground-state exchange interactions while the exciton dispersion is varied to give a best fit to the observed line shapes. The resulting excited-state exchange parameters are shown to be reasonable. The exciton dispersion is found to be quite significant (up to 2 cm^{-1}) for one of the excited states. These two materials thus represent the first examples for which the exciton dispersion of the electronically excited states of a rare-earth salt have been directly observed.

I. INTRODUCTION

In an earlier paper[1] we had suggested that the magnon dispersion was responsible for the unusual line shapes observed in optical transitions originating from the thermally populated magnon state in $GdCl_3$. Here we present more accurate measurements of the line shapes in $GdCl_3$ and similar measurements on $Gd(OH)_3$, both in an external magnetic field of 35 kG along the c axis, which clearly demonstrate the effects of both the magnon and exciton dispersion on the optical properties of these materials.

Previous examples of the influence of the magnons on the optical spectra of magnetically ordered materials have involved studies of the line shapes of spin-wave sidebands accompanying the zero-phonon $\vec{k}=0$ exciton transitions in a diverse group of insulating antiferromagnets. Three types of optical transitions involving the magnon have been observed: (i) the simultaneous creation of a spin deviation and electronic excitation on a pair of ions[2]; (ii) the simultaneous destruction of a thermally populated spin deviation on one ion and the creation of an electronic excitation on another[3]; and (iii) the inverse of process (ii) in fluorescence.[4] In all cases the intensity resulted from the cooperative absorption or emission of more than one ion. However, in the case of $GdCl_3$ and $Gd(OH)_3$ the transition mechanism responsible for the absorption is that of a single ion. A thermally populated spin deviation is destroyed on the same ion which is electronically excited. The interionic interactions lead to dispersion of both the initial and final states resulting in the characteristic line shapes. The situation is somewhat analogous to the band-to-band transitions which have been observed in several organic crystals where the initial phonon state is replaced here by a magnon.[5]

$GdCl_3$ is a ferromagnet whose Curie temperature is 2.20 °K.[6] There have been several attempts to determine the exchange interactions for the ground state of $GdCl_3$ by looking at pairs of Gd^{+3} ions in isostructural hosts and from high-temperature measurements of the specific heat and magnetic susceptibility.[7-11] These have led, until recently, to a range of exchange constants for $GdCl_3$. A recent redetermination of these for $GdCl_3$ by means of high-frequency susceptibility measurements has finally cleared up the disagreements.[12]

The nearest-neighbor (nn) interactions are antiferromagnetic while those of next-nearest neighbors (nnn) are ferromagnetic, the latter dominating. In zero magnetic field the energy gap between the ground state and lowest magnon branch is so small that it is impossible to optically separate transitions from the ground and magnon states. In addition, even at 1.40 °K, the lowest temperature of these experiments, the spin excitations are so highly excited that the spectrum is badly broadened.

Therefore, all optical experiments were performed in a large (35 kG) magnetic field which drives the magnon branches more than 3 cm^{-1} further above the ground state.

$Gd(OH)_3$ was recently shown to order antiferromagnetically at 0.94 °K.[13,14] The nn and nnn exchange interactions have been found to be of the same sign as those of $GdCl_3$. However, unlike $GdCl_3$, the antiferromagnetic nn interactions strongly dominate.[15] The theory upon which we have based our line-shape study assumes a ferromagnetic ground state. $Gd(OH)_3$ is antiferromagnetic; however, in a field of 35 kG the Gd^{+3} spins are almost completely aligned along the field producing a spin configuration identical to that of a ferromagnet. Thus all $Gd(OH)_3$ spectra are taken at 35 kG and the results are analyzed using the spin-wave theory developed for $GdCl_3$.

Using the most recent ground-state exchange constants we have been able to find a unique set of excited-state exchange constants with which we have been able to calculate a weighted combined density-of-states function which fits the observed line shapes exceedingly well. The resulting excited-state exchange interactions are shown to be consistent with some semiquantitative arguments which can be made about the relative magnitude of the exchange in different excited states. With these we have calculated the exciton dispersion curves corresponding to several Gd^{+3} single-ion states. $GdCl_3$ and $Gd(OH)_3$ thus represent two of a small number of magnetic insulators for which it has been possible to determine in detail the dispersion of the optical excitons. Some other examples include Cr_2O_3, discussed by MacFarlane and Allen,[16] and MnF_2, discussed by Meltzer *et al.*[3] However, this work presents the first direct evidence for dispersion of optical excitons in rare-earth insulators.

In Sec. II the experiments are described. Section III develops the theory upon which the optical line shapes were calculated and presents the theoretical relationships expected among the excited-state exchange parameters. In Sec. IV the observed line shapes are described and compared to the theoretical line shapes which best fit them. The resulting excited-state exchange parameters and dispersion curves are presented. In Sec. V the exchange parameters in the different excited states are compared and are shown to be consistent with the theoretically predicted relationships. Finally, the results of this paper are summarized.

II. EXPERIMENTAL

The $Gd(OH)_3$ crystal was grown at Yale University by a method recently described.[17] It was a thin needle with a 0.5-mm optical path and was immersed directly in the liquid-helium bath. Its temperature was determined to ±0.02 °K from the vapor pressure of the helium.

The $GdCl_3$ crystals were grown at Johns Hopkins University by Williams. The crystals ranged in thickness from 0.2 to 2 mm. They were cut and mounted in a dry atmosphere and sealed in a quartz tube filled with half an atmosphere of helium. The tube was immersed directly in the helium bath, but because the sample was not in direct contact with the bath there is a much greater uncertainty in the $GdCl_3$ crystal temperature than for that of $Gd(OH)_3$.

The polarized absorption spectra were recorded photoelectrically with an EMI 9558QB photomultiplier. Due to the high resolution required in these experiments (0.1 cm^{-1} at 32 000 cm^{-1}) the light signal was sufficiently low to require a signal-averaging technique to obtain an adequately high ratio of signal to noise. Light from a 1000-W high-pressure Hg-capillary lamp was passed through the sample after having been predispersed so as to give a 5-Å bandpass. The linearly polarized signal was analyzed with a 1.8-m spectrometer of the Ebert-Fastie design using a 7500-line/in. grating in 20th order. The spectrum was repetitively scanned by rotating the grating with a stepping motor and indexer through a fixed number of steps backwards and forwards. During the forward scan, the amplified photomultiplier signal from each step was digitized and stored in a 1024-channel multichannel analyzer, each step corresponding to a separate channel. After 10–20 scans an adequate signal-to-noise ratio was obtained. Calibration lines from a Fe-Ne hollow-cathode lamp were superimposed on the spectrum.

All spectra were obtained with the crystal in an external magnetic field along the c axis with the light beam perpendicular to the field.

III. THEORY

Here we calculate the line-shape functions for single-ion-induced transitions from the thermally populated magnon state including the dispersion of the electronically excited final states.

In Sec. III A the states of the ^8S and ^6P manifold of the Gd^{+3} ion involved in the optical transitions under study are described. It is shown that even in the C_{3h} site symmetry of the Gd^{+3} ion, M_J can be considered a good quantum number in most of the states of interest.

Section III B describes the magnon and optical-exciton states which are the proper eigenstates of the crystal. Each single-ion state is shown to give rise to a pair of exciton bands. The details of the dispersion of these bands depend predominantly upon the nn (intrasublattice) and nnn (intersublattice) exchange interactions which transfer the excitation (spin or electronic) from one ion to its nn or nnn, respectively. Only the latter splits the pair of bands (Davydov splitting).

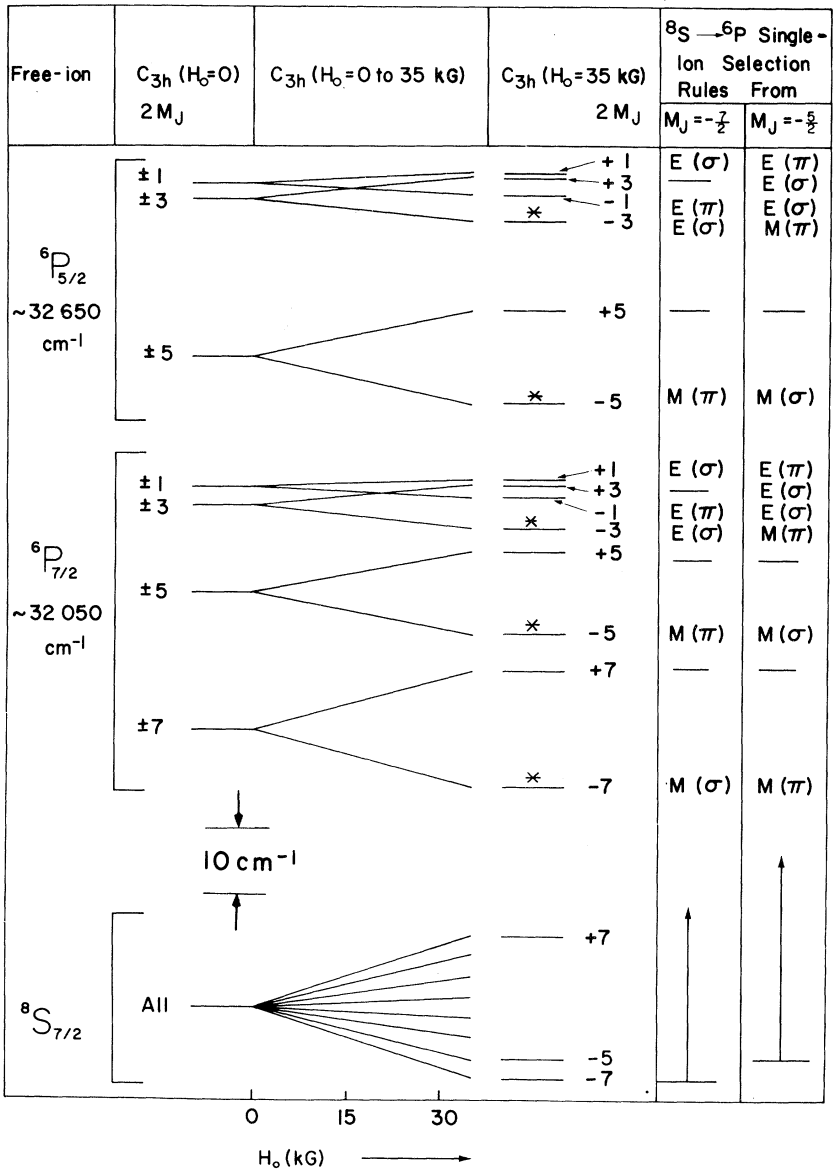

FIG. 1. Effect of a magnetic field along the c axis on the energy levels of the Gd^{+3} ion at a C_{3h} site. The states are labeled by their M_J quantum number. Line shapes of those states marked with an asterisk are discussed in this paper. Single-ion selection rules for transitions to each of the excited states from the ground ($M_J = -\frac{7}{2}$) and magnon ($M_J = \frac{5}{2}$) states are shown on the right-hand side, where M and E signify magnetic and electric dipole active, respectively, and π and σ indicate polarations of $E \| C$, $M \perp C$ and $E \perp C$, $M \| C$, respectively.

In Sec. III C the crystal eigenstates are used to obtain the theoretical absorption coefficient as a function of optical-excitation energy. A basis transformation of the transition-moment operator from the single-ion-state space to the crystal-state space is performed. It is shown that two types of terms arise. The first, which is temperature dependent, allows the destruction of the magnon and the creation of an exciton. The second, which results from the presence of zero-point spin deviations and which is temperature independent, allows the simultaneous creation of an exciton and magnon. The former is responsible for the observed transitions. The line-shape function is then obtained from the transformed transition-moment operator by convoluting it with the combined density of states of the magnon and exciton and with the occupation number of the magnon.

Finally, in Sec. III D the relationships between the excited-state exchange interactions are derived. It is shown that if one assumes pure ^6P character for the electronic single-ion states, the exchange

interactions for states differing in J but with identical M_J are proportional to the square of the Clebsch-Gordan coefficient which couples them to the state $|^6P M_S M_L\rangle$, with $M_S = -\frac{5}{2}$ and $M_L = M_J + \frac{5}{2}$.

A. Single-Ion States

The crystal field states arising from the ^8S and ^6P multiplets of the free ion are split by the spin-orbit coupling into states characterized by a total angular momentum quantum number J as shown in Fig. 1. The L and S character of the states are no longer pure although they are predominantly ^8S and ^6P, respectively.[18]

The C_{3h} site symmetry in these hexagonal salts splits each J manifold into $\frac{1}{2}(2J+1)$ Kramers-degenerate crystal field states. All the low-lying states of the Gd^{+3} ion belong to the half-filled shell ($4f^7$). Since there are no first-order diagonal crystal-field matrix elements between states of a half-closed shell in the limit of Russell-Saunders coupling, the crystal field effects are small in $GdCl_3$ and $Gd(OH)_3$.[19] Hence J remains a useful quantum number.

The crystal-field terms for C_{3h} are such that only those states of $4f^7$ differing in M_J by ± 6 are mixed. Within the ^6P multiplet these include only four states of the $^6P_{7/2}$ manifold. The pairs of mixed states have M_J values $-\frac{7}{2}$, $+\frac{5}{2}$ and $+\frac{7}{2}$, $-\frac{5}{2}$. Since transitions from the ground state (the $M_J = -\frac{7}{2}$ component of $^8S_{7/2}$) to the $M_J = \frac{7}{2}$ or $M_J = \frac{5}{2}$ components of the $^6P_{7/2}$ manifold are forbidden, except as a consequence of their mixing with the $M_J = -\frac{5}{2}$ and $M_J = -\frac{7}{2}$ components of $^6P_{7/2}$, respectively, the appearance of these transitions in the spectrum provides a convincing test of the extent of the mixing.

The low-temperature spectra of $GdCl_3$ and $Gd(OH)_3$ have been reported by Schwiesow and Crosswhite in zero field.[19] The single-ion energy levels for $GdCl_3$ are shown on the left-hand side of Fig. 1. The effect of the external field is also shown, where the splitting factors are those of $LaCl_3 : Gd^{3+}$.[20] Note that in $GdCl_3$ the single-ion states $M_J = \frac{7}{2}$, and $M_J = -\frac{5}{2}$ of $^6P_{7/2}$ are nearly degenerate at 35 kG, as shown on the right-hand side of Fig. 1. As expected, these two states are strongly mixed, as is clearly evident from the appearance of the transition labeled $2M_J = 7$, as the field is increased. Thus for $GdCl_3$, M_J can be considered a good quantum number for all states in the ^6P multiplet except for the $M_J = \frac{7}{2}$ and $M_J = -\frac{5}{2}$ components of $^6P_{7/2}$. For $Gd(OH)_3$ at 35 kG the states are still sufficiently separated in energy (>15 cm^{-1}) so that no significant mixing is evident. Thus in these experiments M_J will be considered pure in all ^6P states of $Gd(OH)_3$.

Since the transition mechanism is that of the single ion, the selection rules will be determined by the C_{3h} site group. These selection rules are[21]

$\Delta M_J = 0(\sigma)$, $\pm 1(\pi)$; magnetic dipole

$\Delta M_J = \pm 2$, $\pm 4(\sigma)$, $\pm 3(\pi)$; electric dipole.

They are summarized on the extreme right-hand side of Fig. 1 for transitions from both the $M_J = -\frac{7}{2}$ and $M_J = -\frac{5}{2}$ components of $^8S_{7/2}$. An asterisk in Fig. 1 indicates this to be a state for which we have studied the line shape. As can be seen, all the transitions whose line shapes have been studied are only magnetic dipole active. This is confirmed by polarization studies of the spectrum, supporting the assumption of a single-ion transition mechanism.

B. Crystal States

$GdCl_3$ and $Gd(OH)_3$ are isostructural crystals belonging to the space group C_{6h}^2.[22,23] The crystal structure is shown in Fig. 2. Each ion has its two nn's located along the c axis with a separation of 4.105 and 3.45 Å in $GdCl_3$ and $Gd(OH)_3$, respectively.[24] Its six nnn's are at the corners of the triangles of Gd^{+3} ions displaced half a unit cell above and below the central Gd^{+3} ion, separated by 4.73 and 4.02 Å for $GdCl_3$ and $Gd(OH)_3$, respectively. Third-nn's are separated by almost twice the nn distances and their exchange interactions will be neglected. This assumption has been confirmed for the ground state.[12,14]

These crystals contain two Gd^{+3} ions in a unit cell. For each single-ion excited state (either a magnon or an exciton), there will be $2N$ degenerate single-ion energy levels corresponding to the $2N$ Gd^{+3} ions in the crystal. The interionic interactions will destroy the degeneracy, resulting in a band of $2N$ crystal states. These states are characterized by the reciprocal-lattice vector $\vec{k}$ so that for each value of $\vec{k}$ there are two crystal ei-

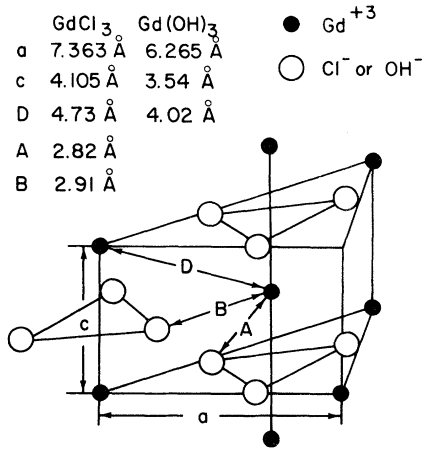

FIG. 2. Crystal structure of $GdCl_3$ and $Gd(OH)_3$.

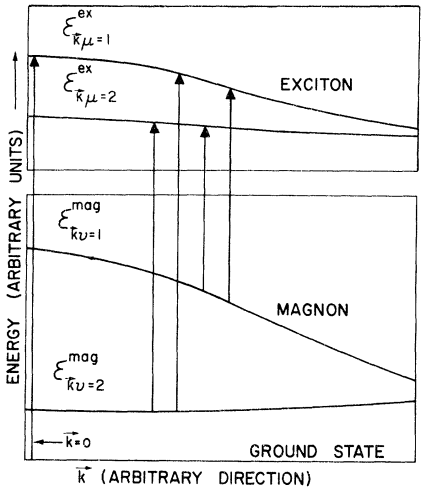

FIG. 3. Typical dispersion curves for the ground, magnon, and exciton states of $GdCl_3$ or Gd $(OH)_3$ along an arbitrary direction in the first Brillouin zone. The vertical arrow on the left indicates the $\vec{k}=0$ transition from the ground state. The four arrows in the middle represent the four interband transitions which can take place for each value of $\vec{k}$.

genstates. A representative set of dispersion curves for the magnon and exciton state are shown in Fig. 3 for an arbitrary direction in the first Brillouin zone. It is these dispersion curves and the resulting crystal eigenstates which we must first determine.

1. Magnon Solution

The magnon problem has already been examined by Marquard and Stinchcombe.[25] Their work will be briefly reviewed. The details can be found in Ref. 25.

Since the Gd^{+3}-ion ground state is $^8S_{7/2}$ the exchange is assumed to be isotropic. In these Gd^{+3} salts, the magnitude of the dipolar and exchange interactions are comparable. Therefore, a Hamiltonian containing terms from both must be simultaneously diagonalized. The dipolar contributions complicate the problem since zero-point effects occur, unlike the case for a purely exchange-coupled Heisenberg ferromagnet. The ground-state Hamiltonian in an external field H_0 along the c axis is

$$\begin{aligned}\mathcal{H} = &-2\sum_{i(p),j(q)} J_{i(p)j(q)}\,\vec{S}_{i(p)}\cdot\vec{S}_{j(q)} \\ &-(g\mu_B)^2[3(\vec{S}_{i(p)}\cdot\vec{r})(\vec{S}_{j(q)}\cdot\vec{r}) \\ &-(\vec{S}_{i(p)}\cdot\vec{S}_{j(q)})r^2]r^{-5} - g\mu_B H_0\sum_{i(p)} S^z_{i(p)}\,, \end{aligned} \tag{1}$$

where $i(p)$ and $j(q)$ signify ions i and j on sublattice p and q, respectively, $\vec{r}=\vec{r}_{i(p)j(q)}$, $J_{i(p)j(q)}$ is the exchange interaction for a pair of ions $i(p)$ and $j(q)$, $\vec{S}_{i(p)}$ is the spin operator of the $i(p)$th ion, g is the g factor of the ground state, and μ_B is the Bohr magneton.

A linear spin-wave theory is now introduced by replacing the single-ion spin operators $\vec{S}_{i(p)}$ by the appropriate single-ion spin creation and destruction operators $a^\dagger_{i(p)}$ and $a_{i(p)}$. Only terms quadratic in the Hamiltonian are retained. Sublattice spin-wave creation and destruction operators defined by

$$\begin{aligned} a^\dagger_{\vec{k}p} &= N^{-1/2}\sum_{i(p)} e^{-i\vec{k}\cdot\vec{l}(p)} a^\dagger_{i(p)}\,, \\ a_{\vec{k}p} &= N^{-1/2}\sum_{i(p)} e^{i\vec{k}\cdot\vec{l}(p)} a_{i(p)} \end{aligned} \tag{2}$$

are now introduced and the resulting Hamiltonian is diagonalized.

Marquard showed that the $\pm\vec{k}$ sublattice modes are coupled. The transformation which diagonalizes the Hamiltonian is

$$\begin{pmatrix} b^\dagger_{\vec{k}} \\ b_{-\vec{k}} \end{pmatrix} = -\begin{pmatrix} \alpha & \beta \\ \gamma & \delta \end{pmatrix}\begin{pmatrix} a^\dagger_{\vec{k}} \\ a_{-\vec{k}} \end{pmatrix},\quad \begin{pmatrix} b^\dagger_{-\vec{k}} \\ b_{k} \end{pmatrix} = -\begin{pmatrix} \delta^* & \gamma^* \\ \beta^* & \alpha^* \end{pmatrix}\begin{pmatrix} a^\dagger_{-k} \\ a_{\vec{k}} \end{pmatrix}, \tag{3}$$

provided the transformation matrices satisfy the eigenvalue equation

$$\begin{aligned} &\begin{pmatrix} \epsilon(\vec{k}) & 0 \\ 0 & -\epsilon(-\vec{k}) \end{pmatrix}\begin{pmatrix} \alpha & \beta \\ \gamma & \delta \end{pmatrix} \\ &\quad = \begin{pmatrix} \alpha & \beta \\ \gamma & \delta \end{pmatrix}\begin{pmatrix} A^*(\vec{k}) & B^*(\vec{k}) \\ -B(-\vec{k}) & -A(-\vec{k}) \end{pmatrix}, \end{aligned} \tag{4}$$

where α, β, γ, δ, A, and B are $\vec{k}$-dependent 2×2 matrices and $\epsilon(\vec{k})$ is the magnon eigenvalue. The matrices A and B can be expressed in terms of the exchange interactions, dipolar interactions, and external magnetic field and are to be found in Ref. 25. The $b^\dagger_{\vec{k}}$ and $b_{\vec{k}}$ are two-dimensional column vectors for the creation and destruction operators of the pair of magnon eigenstates at the reciprocal-lattice point $\vec{k}$. The $a^\dagger_{\vec{k}}$, $a_{\vec{k}}$ are two-dimensional column vectors for the creation and destruction operators for the pair of sublattice magnon states defined in Eq. (2). Analytic expressions for the magnon eigenvalues, which we will make use of later, are also given in Ref. 25.

2. Exciton Solutions

For the electronically excited states a much more general form of the Hamiltonian is chosen than was used in Sec. III A because in general the exchange can be expected to be quite anisotropic. This is a result of a crystalline-field interaction which is much larger than the exchange or dipolar

interactions in the excited states. The Hamiltonian is written

$$\mathcal{H}=\sum_{i(p)}\mathcal{H}_{i(p)}+\tfrac{1}{2}\sum_{i(p)j(q)}V_{i(p)j(q)}\,, \tag{5}$$

where $\mathcal{H}_{i(p)}$ is the Hamiltonian for a single ion subject to the influence of the crystalline and dipolar fields of the other ions and an external magnetic field. $V_{i(p)j(q)}$ is the Coulomb-interaction operator between the $i(p)$th and $j(q)$th ions, one in the ground state and one in an electronically excited state. All exchange interactions coupling different single-ion states are ignored, i.e., the dispersion is that of an energetically isolated nondegenerate single-ion state. The dipolar interaction can be placed in the single-ion Hamiltonian because it will only affect the relative energy of the single-ion states. It will not lead to dispersion in the excited states since it cannot transfer energy between ions when the pair of ions are in states of differing spin multiplicities.

Exchange involving both nn's and nnn's will give rise to dispersion while only the latter will contribute to a splitting of the bands (Davydov splitting[26]).

We start out by defining sublattice exciton creation and destruction operators $A^{\dagger}_{\vec{k}p}, A_{\vec{k}p}$ in a way analogous to the corresponding magnon sublattice operators $a^{\dagger}_{\vec{k}p}$, $a_{\vec{k}p}$ by replacing $a^{\dagger}_{i(p)}$, $a_{i(p)}$ with $A^{\dagger}_{i(p)}$, $A_{i(p)}$ in Eq. (2). $A^{\dagger}_{i(p)}$, $A_{i(p)}$ are the creation and destruction operators for the single-ion electronically excited state. The intersublattice exchange mixes the sublattice excitons giving creation operators which diagonalize the Hamiltonian of the form

$$B^{\dagger}_{\vec{k}\mu}=\sum_{p}\xi_{\mu p}(\vec{k})A^{\dagger}_{\vec{k}p}\,. \tag{6}$$

The $\xi_{\mu p}$'s are found from solutions of the two eigenvalue equations

$$\sum_{q}\left[\Gamma_{pq}(\vec{k})-\delta_{pq}\epsilon^{ex}_{\vec{k}}\right]\xi_{pq}=0\,, \tag{7}$$

with

$$\Gamma_{pq}(\vec{k})=\sum_{j(q)\neq i(p)}e^{i\vec{k}\cdot\vec{r}}\langle i(p)|V_{i(p)j(q)}|j(q)\rangle\,. \tag{8}$$

Here $|i(p)\rangle$ and $|j(q)\rangle$ are states of the crystal in which all the ions are in the ground state except for ion $i(p)$ and $j(q)$, respectively, which are in the single-ion excited state under consideration. By applying the crystal-symmetry operations to the matrix elements of Eq. (8) it can be shown that they are real, that the two matrix elements for nn exchange are equal, and that the six matrix elements for nnn exchange are equal. Performing the summation in Eq. (8) for $GdCl_3$ or $Gd(OH)_3$ one finds

$$\Gamma_{11}(\vec{k})=\Gamma_{22}(\vec{k})=2V_1\cos k_z C\,, \tag{9}$$

$$\Gamma_{12}(\vec{k})=\Gamma^{*}_{21}(\vec{k})=2V_2\cos\frac{k_z c}{2}\times\left[2\cos\frac{k_x a}{2}\exp\left(\frac{-ik_y a}{2\sqrt{3}}\right)+\exp\left(\frac{ik_y a}{\sqrt{3}}\right)\right]\,, \tag{10}$$

where V_1 and V_2 are the nn and nnn exchange matrix elements, respectively.

The eigenvalues of Eq. (7) are

$$\epsilon^{ex}_{\vec{k}1}=\Gamma_{11}(\vec{k})+|\Gamma_{12}(\vec{k})|,\quad \epsilon^{ex}_{\vec{k}2}=\Gamma_{11}(\vec{k})-|\Gamma_{12}(\vec{k})|\,, \tag{11}$$

with the coefficient matrix given by

$$\xi(\vec{k})=(2)^{-1/2}\begin{pmatrix}1 & \Gamma^{*}_{12}/|\Gamma_{12}|\\ \Gamma_{12}/|\Gamma_{12}| & -1\end{pmatrix}. \tag{12}$$

It is seen that the electronic excitation has an equal probability of being found on either sublattice.

C. Line-Shape Function

Since the transition mechanism is that of the single ion, the transition-moment operator is written

$$\vec{M}_f=\vec{m}_f\sum_{i(p)}A^{\dagger}_{f\,i(p)}a_{i(p)}\,, \tag{13}$$

where $\vec{m}_f$ is the single-ion transition moment for an excitation from the first spin excited state of the ground-state manifold to the fth single-ion electronically excited state. $A^{\dagger}_{f\,i(p)}$ is the fth excited-state creation operator on site $i(p)$, and $a_{i(p)}$ is the spin-excitation destruction operator on site $i(p)$. When the interionic interactions are included these excitations are no longer eigenstates of the crystal. The transition-moment operator is therefore transformed to a basis of the crystal-state space.

From the results of Secs. III A and III B, the single-ion electronic-excitation creation operator and spin-deviation destruction operator can easily be expressed in terms of the crystal-state creation and destruction operators. Noting that

$$\sum_{i(p)}A^{\dagger}_{i(p)}a_{i(p)}=\sum_{k,p}A^{\dagger}_{\vec{k}p}a_{\vec{k}p} \tag{14}$$

and using the inverse of the transformations given in Eqs. (3) and (6), i.e.,

$$R(\vec{k})=\begin{pmatrix}\delta^{*} & \gamma^{*}\\ \beta^{*} & \alpha^{*}\end{pmatrix}^{-1},\quad S(\vec{k})=\xi(\vec{k})^{-1}\,, \tag{15}$$

one can write

$$\sum_{i(p)}A^{\dagger}_{i(p)}a_{i(p)}=\sum_{\vec{k}}\sum_{\mu,\nu}\left[(S_{1\mu}R_{3t}+S_{2\mu}R_{4t})B^{\dagger}_{\vec{k}\mu}b_{\vec{k}\nu}+(S_{1\mu}R_{3\nu}+S_{2\mu}R_{4\nu})B^{\dagger}_{\vec{k}\mu}b^{\dagger}_{-\vec{k}\nu}\right]\,, \tag{16}$$

with $t=\nu+2$. The terms involving $B^{\dagger}_{k\mu}b_{\vec{k}\nu}$ destroy

a magnon and create an exciton both of wave vector $\vec{k}$, whereas the terms $B^{\dagger}_{\vec{k}\mu} b^{\dagger}_{\vec{k}\nu}$ simultaneously create both an exciton and a magnon of opposite wave vectors. In this paper we shall be concerned with the terms $B^{\dagger}_{\vec{k}\mu} b_{\vec{k}\nu}$. However, there is considerable evidence that a weak absorption on the high-energy side of the transition to the $\vec{k}=0$ exciton state is described by the term $B^{\dagger}_{\vec{k}\mu} b^{\dagger}_{\vec{k}\nu}$. Its presence implies that a spin-wave sideband involving the simultaneous creation of an exciton and magnon (usually thought of as a two-ion process) can result from a single-ion transition mechanism in the case of a ferromagnet with zero-point spin deviations. This will be the subject of another paper.

The four $B^{\dagger}_{\vec{k}\mu} b_{\vec{k}\nu}$ terms of Eq. (16) can be easily visualized. Consider the representative dispersion curves for the magnon and exciton shown in Fig. 3. Similar curves can be drawn for other directions in the zone. Note that for each value of $\vec{k}$, two crystal eigenstates occur each for the magnon and exciton. Only transitions which conserve $\vec{k}$ can occur because the optical electromagnetic radiation which induces the transitions has a long wavelength compared to the lattice spacings ($\vec{k}_{\text{light}} \approx 0$). This means that only vertical transitions can occur. Thus for each value of $\vec{k}$ four transitions are possible as indicated by the four vertical lines in the middle of Fig. 3. Each transition corresponds to one of the four terms $B^{\dagger}_{\vec{k}\mu} b_{\vec{k}\nu}$ appearing in Eq. (16).

To determine the line-shape functions one must randomly sum over all points in the Brillouin zone. Each point will give rise to four possible transitions, each contributing an intensity proportional to the square of the transition moment for that term $B^{\dagger}_{\vec{k}\mu} b_{\vec{k}\nu}$ of Eq. (16). Because the magnon is thermally populated, each term must be multiplied by the occupation number for the magnon $\langle n_{\vec{k}\nu} \rangle$. Denoting the exciton and magnon energies by $\epsilon^{\text{ex}}_{\vec{k}\mu}$ and $\epsilon^{\text{mag}}_{\vec{k}\nu}$ the line-shape function can be written

$$\alpha(\epsilon) = C\,|\vec{m}_f|^2 \sum_{\vec{k}} \sum_{\mu,\nu} \left[|S_{1\mu} R_{3t} + S_{2\mu} R_{4t}|^2 \langle n_{\vec{k}\nu} \rangle \times \delta(\epsilon - \epsilon^{\text{ex}}_{\vec{k}\mu} + \epsilon^{\text{mag}}_{\vec{k}\nu}) \right], \quad (17)$$

with $t = \nu + 2$ and

$$\langle n_{k\nu} \rangle = [\exp(\epsilon^{\text{mag}}_{\vec{k}\nu}/kT) - 1]^{-1}\ ; \quad (18)$$

C is a constant which will depend on the multipole character of the transition mechanism.

D. Relationship among Excited-State Exchange Interactions

The exchange matrix elements responsible for the exciton dispersion are $\langle i(p)|V_{i(p)j(q)}|j(q)\rangle$, where $|i(p)\rangle$ is a crystal state corresponding to the single-ion excited state f defined by

$$|i(p)\rangle = |f_{i(p)} \prod_{j(q)\neq i(p)} g_{j(q)}\rangle\ . \quad (19)$$

Here g denotes the ground state. The electrons are properly antisymmetrized among all the ions. Because the interaction is a two-ion process, the matrix elements are simply

$$\langle f_{i(p)} g_{j(q)} | V_{i(p)j(q)} | g_{i(p)} f_{j(q)} \rangle\ . \quad (20)$$

The single-ion excited states being considered are all crystal-field components of ^6P_J with $J = \frac{7}{2}, \frac{5}{2}$. As noted previously, J can be considered a good quantum number in all the states under consideration. This is also true of M_J in all but one excited state under study. With the exception of this state, the single-ion excited states may be denoted by $|J, M_J\rangle$. These are linear combinations of the states $|LSJM_J\rangle$, where the coefficients $C(LSJ)$ have been determined for the free ion by Wybourne.[18] Further expanding the states $|LSJM_J\rangle$ in the basis $|SLM_S M_L\rangle$ using the Clebsch-Gordan coefficients $\langle SLM_S M_L | SLJM_J\rangle$, these can be written

$$|JM_J\rangle = \sum_{LS} C(SLJ) \sum_{M_L M_S} \langle SLM_S M_L | SLJM_J\rangle |SLM_S M_L\rangle. \quad (21)$$

In the $SLM_S M_L$ scheme the ground state is to a good approximation

$$|g\rangle = |\tfrac{7}{2}0 - \tfrac{7}{2}0\rangle\ . \quad (22)$$

Substituting Eq. (21) into Eq. (20) the excited-state interaction matrix elements are

$$\sum_{LL';SS'} C(SLJ)C'(S'L'J) \sum_{M_L M'_L; M_S M'_S} \langle SLM_S M_L | SLJM_J\rangle \langle S'L'M'_S M'_L | S'L'JM_J\rangle \times \langle (SLM_S M_L)_{i(p)} (g)_{j(q)} | V_{i(p)j(q)} | (g)_{i(p)} (S'L'M'_S M'_L)_{j(q)} \rangle\ . \quad (23)$$

Since $V_{i(p)j(q)}$ is a spin-independent operator, $M_S = M'_S$ so that the total spin projection along the c axis is conserved. Since $V_{i(p)j(q)}$ is a two-electron operator, only one unit of spin may be interchanged between a pair of ions. Hence $M_S = M'_S = -\frac{7}{2} \pm 1$. Since octet is the highest multiplicity available, $M_S = M'_S = -\frac{5}{2}$. In order that the Clebsch-Gordan coefficient not vanish, $M'_L = M_L = M_J + \frac{5}{2}$. Denoting $M_J + \frac{5}{2}$ by M, the interaction matrix element is now

$$\sum_{LL';SS'} C(SLJ)C'(S'L'J)\langle SL-\tfrac{5}{2}M\,|\,SLJM_J\rangle\langle S'L'-\tfrac{5}{2}M\,|\,S'L'JM_J\rangle \times\langle(SL-\tfrac{5}{2}M)_{i(p)}(g)_{j(q)}\,|\,V_{i(p)j(q)}\,|\,(g)_{i(p)}(S'L'-\tfrac{5}{2}M)_{j(q)}\rangle\ . \quad (24)$$

In the limit that the state under study is pure ^6P this reduces to

$$\langle\tfrac{5}{2}1-\tfrac{5}{2}M\,|\,\tfrac{5}{2}1JM_J\rangle^2\langle(\tfrac{5}{2}1-\tfrac{5}{2}M)_{i(p)}(g)_{j(q)}\,|\times V_{i(p)j(q)}|(g)_{i(p)}(\tfrac{5}{2}1-\tfrac{5}{2}M)_{j(q)}\rangle\ . \quad (25)$$

Note that the Coulomb matrix element is independent of J. Hence the magnitude of the exchange interactions for states of different J and the same M_J are proportional to the square of the Clebsch-Gordan coefficients.

If, in addition, the Coulomb matrix elements are treated as being roughly the same order of magnitude, independent of M_J, then the magnitude of all the excited-state exchange interactions are, crudely speaking, proportional to the squares of the Clebsch-Gordan coefficients. These are tabulated in Table I.

IV. FITTING OBSERVED LINE SHAPES

The absorption coefficient was calculated from Eq. (17). The ground-state exchange constants, which were chosen from those most recently reported in the literature, determine the matrix $R(\vec{k})$ and the eigenvalues $\epsilon^{\rm mag}_{\vec{k}\nu}$. The excited-state exchange constants, which were varied to provide a best fit to the observed line shape, determine $S(\vec{k})$ and $\epsilon^{\rm ex}_{\vec{k}\mu}$.

For these calculations the external field was replaced by an effective local field $H_{\rm eff}$,

$$H_{\rm eff}=H_0+M_0(\tfrac{4}{3}\pi-N_z)\ , \quad (26)$$

where M_0 is the sample magnetization and M_0N_z is the demagnetizing field along the c axis. This was necessary because the dipole-wave sums were determined over a sphere. To this must be added the Lorentz and demagnetizing fields to account for the true sample shape. The samples considered in this paper were either flat plates ($GdCl_3$) or needless [$Gd(OH)_3$]. Because of their orientation in these experiments the demagnetizing field was small [$N_z\approx(4\pi)^{-1}$].

The sum in Eq. (17) was taken over 4000 randomly selected points over the Brillouin zone. The contribution to the line shape function from each term in the sum was given a Gaussian distribution about its value of the transition energy ϵ. This was done because the line shape of the $\vec{k}=0$ transition from the crystal ground state to each exciton state, although very sharp, has a half-width which is not negligible compared to that of the corresponding transition from the magnon state. Since this transition represents approximately the contribution of one point in the Brillouin zone, a similar distribution was chosen for each term in the sum of the line-shape function. The half-width, $\Delta\epsilon_{1/2}$, was selected to give a best over-all fit of the line shape and in all cases turned out to be not more than a factor of 2 different from the half-width of the transition to the $\vec{k}=0$ exciton state.

TABLE I. Square of some relevant Clebsch-Gordan coefficients compared to the exchange parameters which give a best fit to the observed line shapes.

State	Square of Clebsch-Gordan coefficient[a]	$GdCl_3$			$Gd(OH)_3$ Set 1		$Gd(OH)_3$ Set 2		
$^6P_JM_J$	$\langle\frac{5}{2}1-\frac{5}{2}M\,\vert\,\frac{5}{2}1JM_J\rangle^2$	V_1[b,c]	V_2[b,c]	$\Delta\epsilon_{1/2}$[c]	V_1[b,c]	V_2[b,c]	V_1[b,c]	V_2[b,c]	$\Delta\epsilon_{1/2}$[c]
$^6P_{7/2}-\frac{7}{2}$	1	0.21	−0.02	0.54	0.40	0.04	0.34	0	0.54
$^6P_{5/2}-\frac{5}{2}$	$\frac{5}{7}$	−0.08[d]	−0.02	0.54	....	...	...	...	...
$^6P_{5/2}-\frac{3}{2}$	$\frac{2}{7}$	0.08	−0.02	0.40	0.10	0.02	0	0	0.80
$^6P_{7/2}-\frac{5}{2}$	$\frac{2}{7}$	−0.03[d]	0.01	0.27	0.01	0.03	−0.08	0	0.54
$^6P_{7/2}-\frac{3}{2}$	$\frac{1}{21}$	0.01	−0.02	0.54	−0.02	0.02	−0.12	0	0.67
$^8S_{7/2}-\frac{5}{2}$[e]	...	0.19	−0.23	...	0.44	−0.04	0.36	−0.08	...

[a] Note that $M=M_J+\frac{5}{2}$.
[b] Units of cm^{-1}.
[c] The uncertaintities in these exchange interactions are estimated as V_1 (±0.04 cm^{-1}) and V_2 (±0.03 cm^{-1}).
[d] The observed ratio of V_1 and V_2 for this pair of states is expected to be less than 2.5:1 because M_J is not a good quantum number. The state $^6P_{7/2}-\frac{5}{2}$ couples to $^6P_{7/2}\,\frac{7}{2}$, which cannot transfer energy with an ion in the ground state.
[e] Because of the different choice of Hamiltonian for the magnon and exciton states, $V_i=-7J_i$ ($i=1,2$).

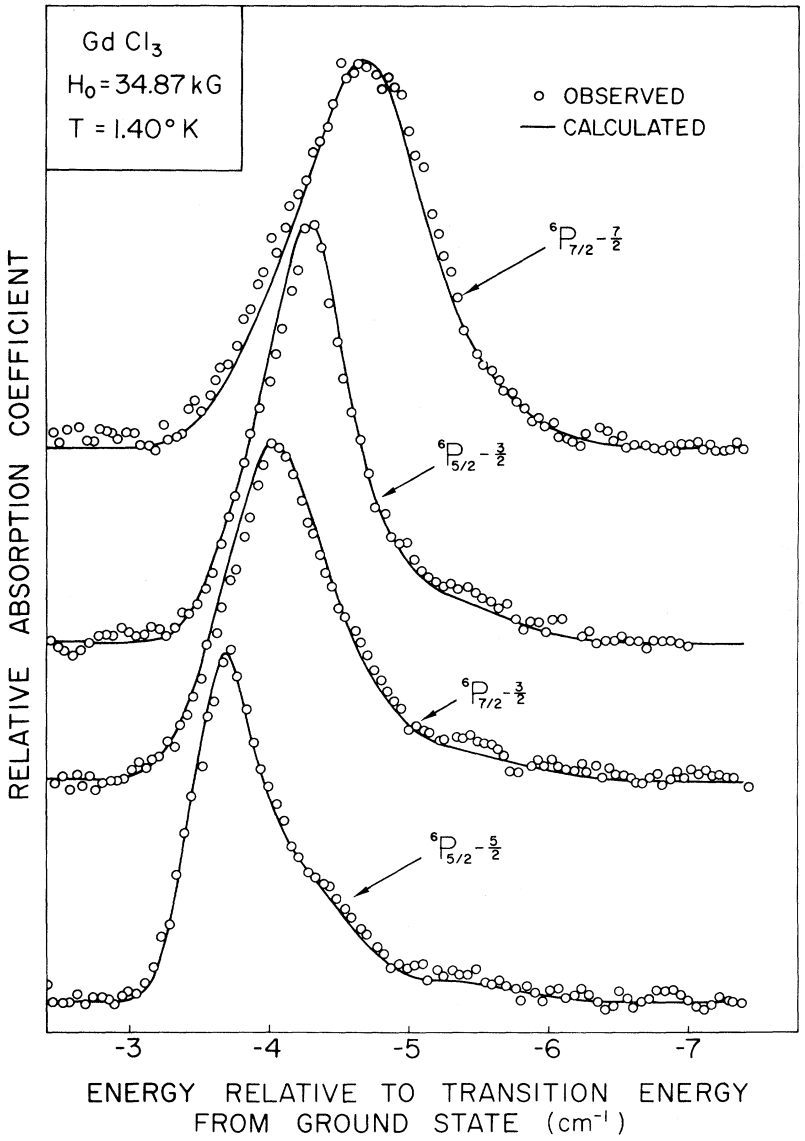

FIG. 4. Line shapes for the magnon-exciton absorption in $GdCl_3$ at 1.40 °K in a magnetic field of 34.87 kG along the c axis. The relative absorption coefficients for different transitions are not to scale. The solid curves are the calculated line shapes with the exchange parameters listed in Table I.

A. $GdCl_3$

The observed line shapes for all states whose line-shapes were studied, except the ${}^6P_{7/2}M_J = -\frac{5}{2}$ excited state, are shown in Fig. 4.[27] All experiments were performed at 1.40 °K in a field of 34.87 kG directed along the c axis. The ground-state exchange parameters are those of Clover and Wolf[12]: $J_1 = -0.0271$ cm^{-1}, $J_2 = 0.0333$ cm^{-1}. Having chosen these, it is possible to find a unique set of excited-state exchange parameters that result in a calculated line shape shown by the solid lines in Fig. 4. These describe very well the observed line shapes and their positions relative to the corresponding transition from the ground state. In these fits no attempt has been made to calculate the absolute magnitude of the absorption coefficients. The resulting exchange parameters are consistent with the results of Sec. III D and are discussed in Sec. V.

In Fig. 5 is shown the first Brillouin zone of the $GdCl_3$ and $Gd(OH)_3$ crystal. The calculated magnon and exciton dispersion curves of $GdCl_3$ along several special directions of the zone appear in Fig. 6 for a crystal in a magnetic field of 34.87 kG along the c axis.

Although the dispersion of the exciton states is much smaller than the magnon dispersion, it is not insignificant, particularly for the lowest-energy exciton (1 cm^{-1}). Note that the intrasublattice excited-state exchange is so small (< 0.25 cm^{-1}) that the two exciton branches are nearly degenerate at all points in the Brillouin zone (i.e., small Daydov splittings).

By looking at the dispersion curves of Fig. 6 it is easy to see why the positions of the transitions from the magnon to the different excited states are shifted by different amounts relative to the corresponding transitions from the ground state. The transition from the ground state terminates on the upper $\vec{k}=0$ exciton branch. The transition from the magnon state can originate with any value of $\vec{k}$. However, the $\vec{k}$ value of the exciton which is excited must be identical to the $\vec{k}$ value of the initial magnon state. When there is no exciton dispersion the transition from the magnon state is displaced relative to the corresponding transition from the ground state by an energy equal to the magnon energy. The peak of the line shape occurs where the thermally weighted magnon density of states is greatest which is near the top face of the Brillouin zone (A point). This is the case for several of the higher-energy excitons (see Fig. 4). However, for ${}^6P_{7/2}M_J=-\frac{7}{2}$ the exciton energy for the top face of the zone is lowered relative to the $\vec{k}=0$ state due to the exchange interaction. The absorption peak is therefore further displaced in energy from the corresponding transition from the ground state and the line shape is altered.

B. $Gd(OH)_3$

The observed line shapes are shown in Fig. 7. The experimental conditions were the same as those of $GdCl_3$, except that the $Gd(OH)_3$ crystals were immersed directly in the liquid helium. The ground-state exchange parameters are essentially those of Cochrane, Wu, and Wolf[15] with $J_1=-0.0626$ cm^{-1} and $J_2=0.0059$ cm^{-1} (set 1). By varying the excited-state exchange parameters, the best calculated line shapes are shown by the solid curves of Fig. 7. Note that the calculated line shapes underestimate the low-energy portion of the absorption. By varying both the ground- and excited-state exchange parameters, subject of course to the condition that the ground-state parameters must be identical for all line shapes, the fit can be greatly improved as shown by the broken curve in Fig. 7 for the exchange parameters $J_1=-0.052$ cm^{-1} and $J_2=0.011$ cm^{-1} (set 2). However, as suggested in Sec. V, set 2 does not appear reasonable because the excited-state exchange parameters which it necessitates are inconsistent with the results of Sec. IIID. The dispersion curves from set 1 are shown in Fig. 8 for $H_0=34.87$ kG. Note that the dispersion curves of the lowest exciton (width 2 cm^{-1}) and magnon are quite similar, the latter being 50% larger. Note that these dispersion curves do not represent

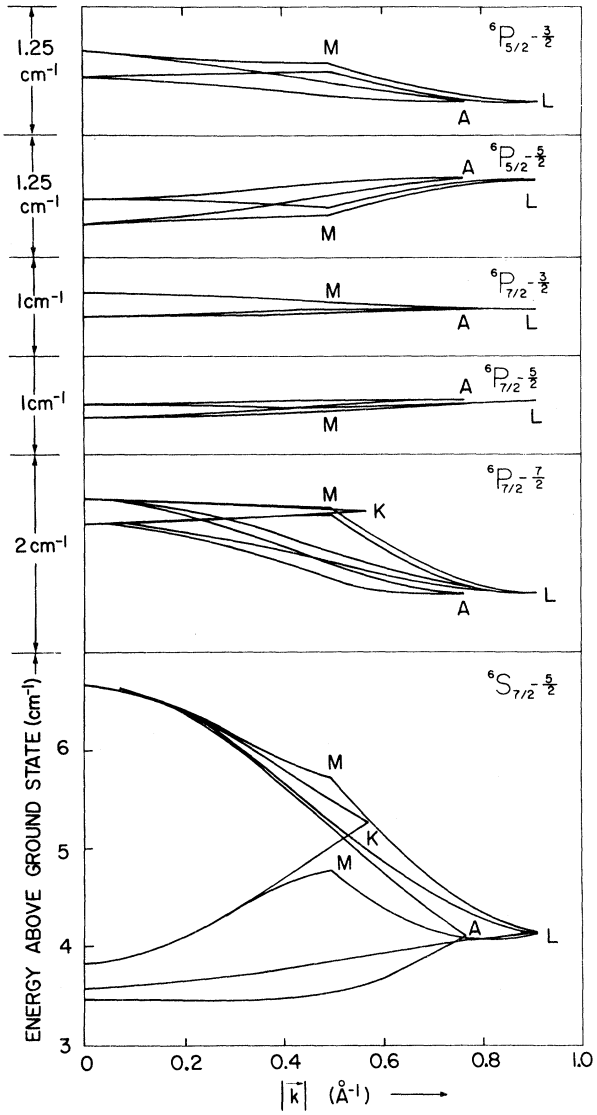

FIG. 6. Energy dispersion curves for the magnon and several exciton states of $GdCl_3$ for $\vec{k}$ along some special directions in the first Brillouin zone. The magnetic field is 34.87 kG.

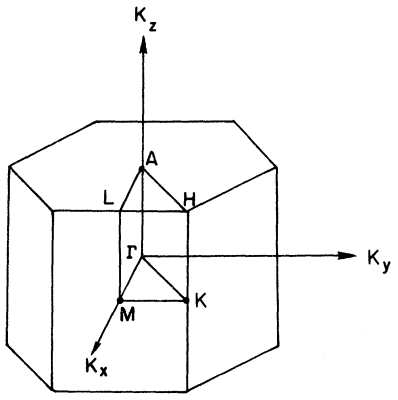

FIG. 5. First Brillouin zone of $GdCl_3$ or Gd $(OH)_3$ with special points marked.

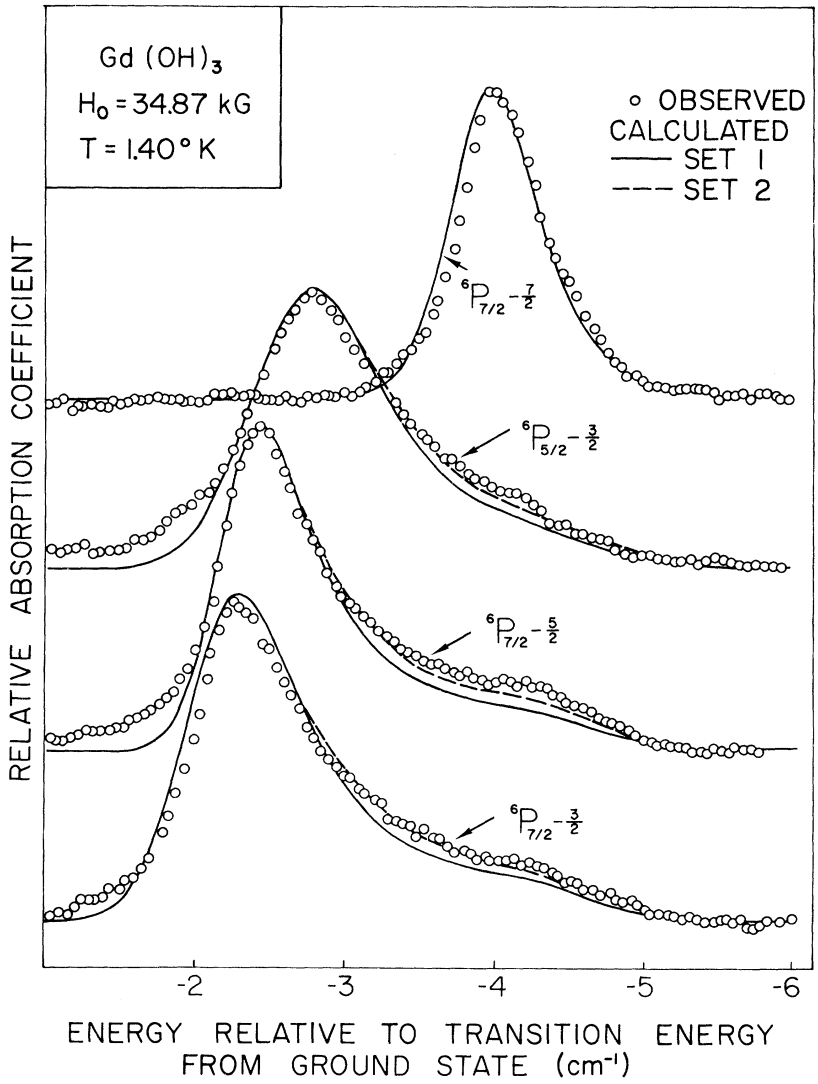

FIG. 7. Line shapes for the magnon-exciton absorption in Gd $(OH)_3$ at 1.40 °K in a magnetic field of 34.87 kG along the c axis. The relative absorption coefficients for different transitions are not to scale. The line shapes were calculated for two different sets of ground- and excited-state exchange parameters: set 1 (solid curve) and set 2 (dashed curve). The exchange parameters are listed in Table I.

those of $Gd(OH)_3$ in its antiferromagnetic state.

As can be seen in Fig. 9, when the temperature is increased from 1.40 to 2.04 °K, the absorption coefficient increases, but not nearly as rapidly as expected. This is also found for $GdCl_3$. This discrepancy remains, at this point, unexplained. Because of the low magnon energy for $Gd(OH)_3$ ($\epsilon = 2$ cm^{-1}, Fig. 8) at the top of the Brillouin zone, where the density of states is relatively high, it is possible that at 34.87 kG and 2.04 °K there are simply too many magnons present to make a noninteracting spin-wave theory adequate. $GdCl_3$ at 34.87 kG should be relatively free of this complication because of the higher energy and different shape of its dispersion curve. However, because of its hygroscopic nature, no experiments on it immersed directly in the helium bath have yet been performed.

V. SUMMARY AND CONCLUSIONS

The excited-state exchange parameters are summarized in Table I. In this table the states are arranged in order of decreasing values of the square of the Clebsch-Gordan coefficient which couples it to the state $|{}^6P M_S M_L\rangle$, with $M_S = -\frac{5}{2}$ and $M_L = M_J + \frac{5}{2}$. According to the discussion of Sec. III D we qualitatively expect the magnitude of the excited-state exchange parameters to fall as the square of Clebsch-Gordan coefficient. With regard to the intrasublattice exchange interaction V_1, this general trend is quite evident. The intersublattice exchange parameter V_2 is found to be so small in all excited states that such a comparison would be of doubtful significance. Note that the exchange parameters for $Gd(OH)_3$ are on the average considerably larger than those of

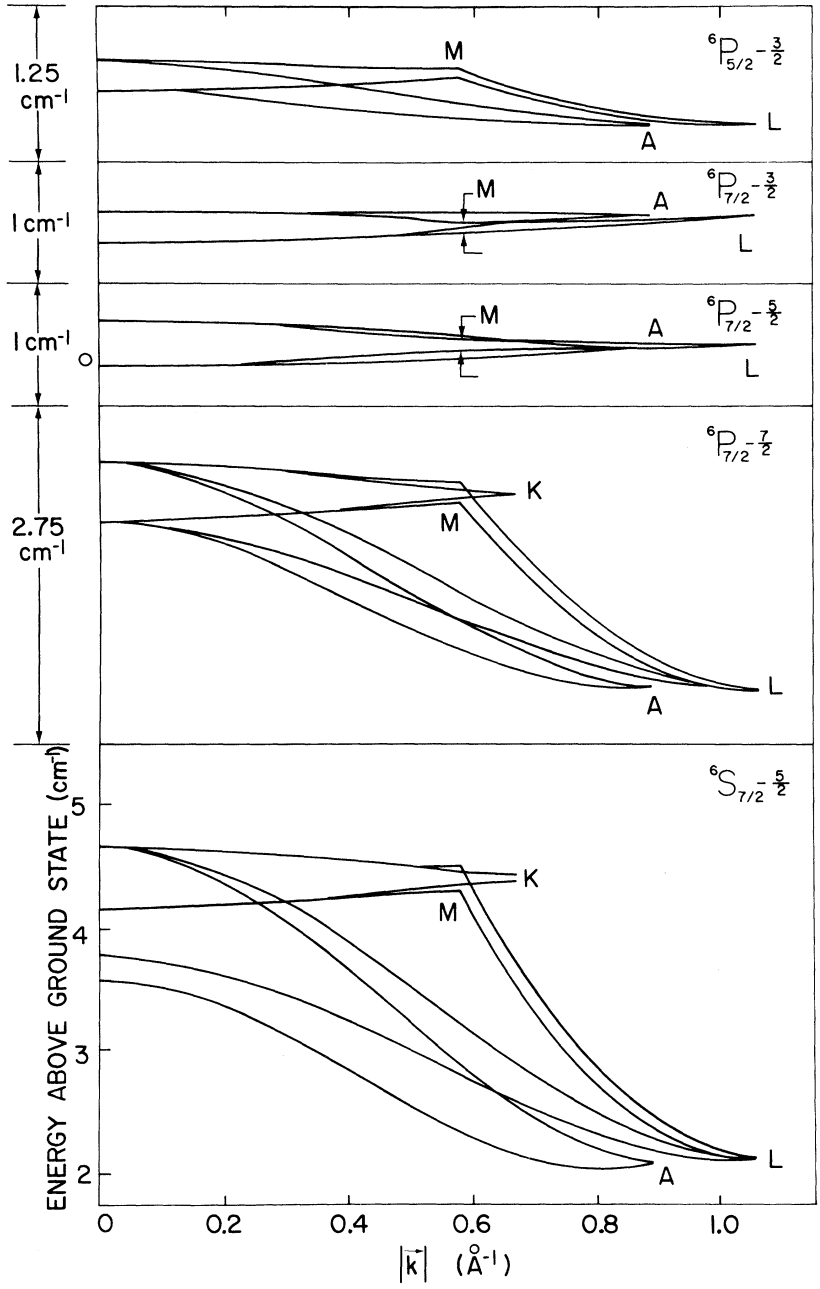

FIG. 8. Energy dispersion curves for the magnon and several exciton states of Gd $(OH)_3$ for $\vec{k}$ along some special directions in the first Brillouin zone. The magnetic field is 34.87 kG.

$GdCl_3$.

One can also compare the ratio of V_1 or V_2 for states of identical M_J and differing J. The predicted ratio as discussed in Sec. IID, under the assumption of pure ^6P character of the states, is shown next to the brackets in column 2 of Table I. These ratios are fairly well borne out for V_1 in $GdCl_3$. The magnitude of V_2 is too small to make a comparison significant.

With regard to $Gd(OH)_3$, only the ratio of V_1 for the states of $M_J=\frac{3}{2}$ can be examined.[28] For the parameters of set 2, this ratio is inverted with regard to what is expected according to Sec. IID. This suggests that an attempt to modify the ground-state exchange parameters is the wrong approach to improve the line-shape fit. For set 1 the ratio is reasonable. The fact that it is of the wrong sign is probably only a result of the small magnitude of V_1 for $|^6P_{7/2}M_J=\frac{3}{2}\rangle$. It is within the uncertainties of these results (± 0.04 cm^{-1}) that it could have a small positive value.

The last row of Table I summarizes the ground-state exchange parameters. Of all states examined in both materials, only the ground state of $GdCl_3$

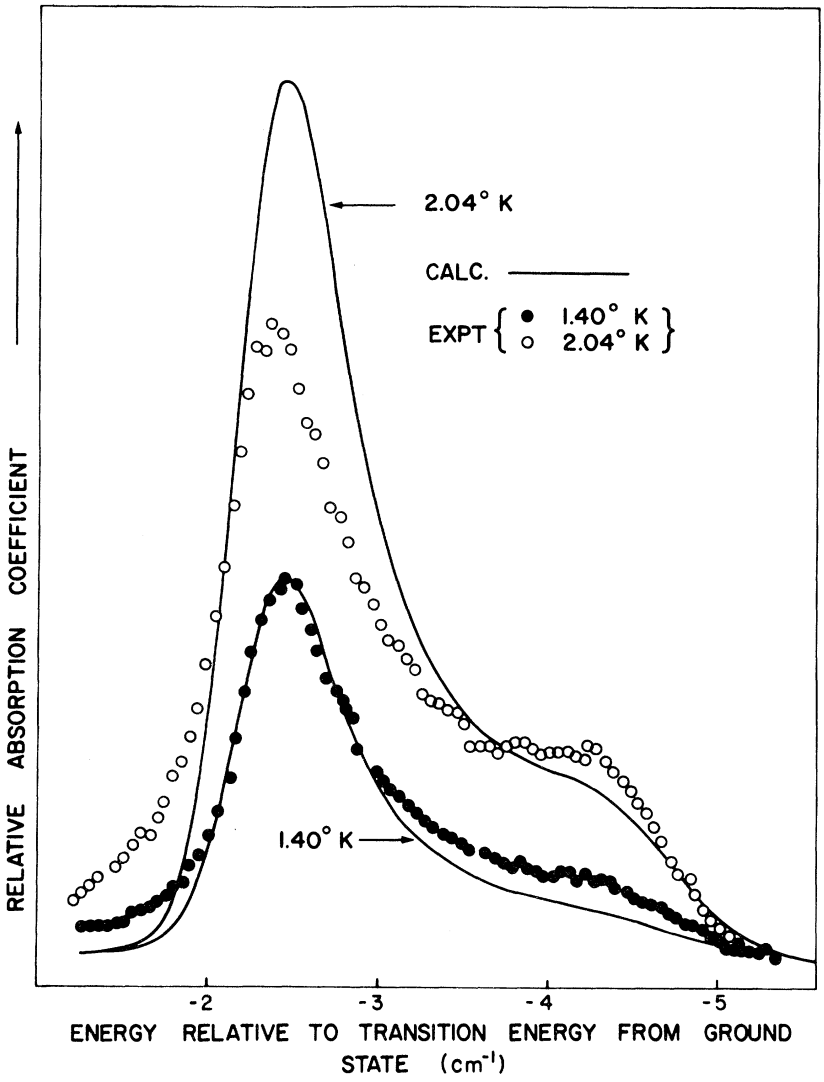

FIG. 9. Calculated (set 1) and observed line shapes for the magnon-exciton ($^6P_{7/2}$-$\frac{5}{2}$) transition in Gd $(OH)_3$ at 1.40 and 2.04°K. The relative absorption coefficients of the calculated line shape were normalized to the peak of the observed line shape at 1.40°K.

shows an appreciable intersublattice exchange parameter.[29] It is J_2 which induces the ferromagnetic ordering of $GdCl_3$. Having now determined the excited-state exchange parameters, the different ground-state properties of $GdCl_3$ and $Gd(OH)_3$ appear even more striking in view of the similar excited-state exchange parameters in the two materials. Note, for instance, the similar shapes of the exciton dispersion curves of $GdCl_3$ and $Gd(OH)_3$ when compared state by state for all but the ground state.

In this paper it has been shown that even in a rare-earth insulating salt, where the single-ion description of the optical properties should have its greatest success, the exciton nature of the ground and excited states is clearly evident in its high-resolution optical spectra. The line shapes of the transitions between these crystal states can be described on the assumption of nn and nnn exchange interactions, with the former dominating except for the $GdCl_3$ ground state. As a result, all exciton dispersion curves are nearly degenerate throughout the Brillouin zone (small Davydov splittings). In general, the exchange interactions of $Gd(OH)_3$ are found to be somewhat larger than the corresponding interactions of $GdCl_3$. The relative magnitude of the excited-state exchange parameters are consistent with some semiquantitative arguments which can be made on the basis of the spin-selection rules on the exchange matrix elements.

Two experimental points which remain to be examined further are (i) the dependence of the absorption strength on temperature and (ii) the possibility that some weak absorption on the high-energy side of the $\vec{k}=0$ exciton line might result from the zero-point spin deviations. These experiments are being planned.

*Work supported by the U. S. Army Research Office, Durham, N. C.

[1]R. S. Meltzer and H. W. Moos, Phys. Rev. Letters 21, 1690 (1968).

[2]A review article on the subject through 1967 is given by D. D. Sell, J. Appl. Phys. 39, 1030 (1968).

[3]R. S. Meltzer, M. Lowe, and D. S. McClure, Phys. Rev. 180, 561 (1968).

[4]R. E. Dietz, A. E. Meixner, H. J. Guggenheim, and A. Misetich, Phys. Rev. Letters 21, 1067 (1968).

[5]S. D. Colson, D. M. Hanson, R. Kopelman, and G. W. Robinson, J. Chem. Phys. 48, 2215 (1968).

[6]W. P. Wolf, M. J. M. Leask, B. Mangum, and A. F. G. Wyatt, J. Phys. Soc. Japan 17, 487 (1961).

[7]E. L. Boyd and W. P. Wolf, J. Appl. Phys. 36, 1027 (1965).

[8]R. J. Birgeneau, M. T. Hutchings, and W. P. Wolf, Phys. Rev. Letters 17, 308 (1966).

[9]R. J. Birgeneau, M. T. Hutchings, and W. P. Wolf, J. Appl. Phys. 38, 957 (1967).

[10]C. D. Marquard, Proc. Phys. Soc. (London) 92, 650 (1967).

[11]M. T. Hutchings, R. J. Birgeneau, and W. P. Wolf, Phys. Rev. 168, 1026 (1968).

[12]R. B. Clover and W. P. Wolf, Solid State Commun. 6, 331 (1968).

[13]H. E. Meissner, thesis (Yale University, 1968) (unpublished).

[14]C. A. Catanese, thesis (Yale University, 1968) (unpublished).

[15]R. W. Cochrane, C. Y. Wu, and W. P. Wolf, J. Appl. Phys. 42, 1568 (1971).

[16]R. M. MacFarlane and J. W. Allen, Phys. Rev. B 4, 3054 (1971).

[17]S. Mroczkowski, J. Eckart, H. Meissner, and J. C. Doran, J. Cryst. Growth 6, 477 (1970).

[18]B. G. Wybourne, Phys. Rev. 148, 317 (1966).

[19]R. L. Schwiesow and H. M. Crosswhite, J. Opt. Soc. Am. 59, 592 (1969).

[20]G. H. Dieke, in *Spectra and Energy Levels of Rare Earth Ions in Crystals*, edited by H. M. Crosswhite and Hannah Crosswhite (Wiley-Interscience, New York, 1968), p. 250.

[21]B. G. Wybourne, *Spectroscopic Properties of Rare Earth Ions* (Wiley-Interscience, New York, 1965), p. 207.

[22]D. H. Templeton and C. H. Dauben, J. Am. Chem. Soc. 76, 5237 (1954).

[23]R. Fricke and A. Seitz, Z. Anorg. Allgem. Chem. 254, 107 (1947).

[24]These values are slightly different than those most recently reported (see Ref. 17). However, the differences should have a negligible effect upon the results of this paper.

[25]C. D. Marquard and R. B. Stinchcombe, Proc. Phys. Soc. (London) 92, 665 (1967).

[26]For a discussion of the Davydov splitting of excitons, see, D. S. McClure, in *Solid State Physics*, edited by F. Seitz and D. Turnball (Academic, New York, 1968), Vol. 8, p. 4.

[27]The line shape of this state is not shown because in the 35 kG of these experiments it overlaps the transition to the ${}^6P_{7/2}M_J=\frac{7}{2}$ state which has been induced by its near degeneracy with ${}^6P_{7/2}M_J=-\frac{5}{2}$. This state was, however, examined at lower magnetic fields.

[28]The line shape of the ${}^6P_{5/2}$-$\frac{5}{2}$ state could not be examined because the transition from the ground state to the $\vec{k}=0$ exciton could not be observed.

[29]If the ground-state Hamiltonian had been written in the same form as that of the excited states the resulting exchange parameters V_i would be related to those of J_i by $V_i=-7J_i$.

PHYSICAL REVIEW B VOLUME 6, NUMBER 1 1 JULY 1972

Method for Determining Minimum-Energy Spin Configurations in a Magnetic Field

H. W. Broughton and William J. Mullin

Department of Physics and Astronomy, University of Massachusetts, Amherst, Massachusetts 01002

(Received 21 January 1972)

The Luttinger-Tisza method of finding minimum-energy spin configurations is generalized to include cases in which an external magnetic field is present. Several examples are given to illustrate the uses and limitations of the method.

I. INTRODUCTION

The purpose of this paper is to present an extension of the Luttinger-Tisza (LT) method of finding minimum-energy spin configurations to the case in which a magnetic field is present. The LT method was originally developed[1] to treat the case of interacting one-dimensional dipoles on a three-dimensional lattice. Luttinger[2] later applied the technique to Ising-model spin systems. Lyons and Kaplan[3] were the first to consider the method in application to three-dimensional spin vectors and they also generalized it to the case of a system containing several types of inequivalent spins. These authors used the LT method to provide a rigorous proof that the ground state of a system of equivalent spins is a spiral. The LT method, has since been used in a wide variety of applications.[4] The reader is referred to the article by Keffer[5] for a review and for references to other